JOURNAL OF AIRCRAFT
Vol. 33, No. 5, September–October 1996

Development of a Finite Element Aeroelastic Analysis Capability

K. K. Gupta*
NASA Dryden Flight Research Center, Edwards, California 93523

Extensions of the general-purpose finite element (FE) structural analysis program STARS for computational fluid dynamics (CFD) based aeroelastic analysis are described. Previous capabilities include structural as well as aeroelastic and aeroservoelastic analyses using linear aerodynamic theories. The current extension involves FE-based CFD solution techniques for aeroelastic analysis, and this article describes the development and application of this integrated, multidisciplinary FE analysis tool for effective modeling and simulation of aerospace vehicles. Numerical examples of flutter solution of two representative problems, namely a panel and a 45-deg swept-back wing are presented in this article, along with comparisons of computed and experimental results that testify to the efficacy of the presently developed numerical techniques.

Nomenclature

$\hat{C}$ = generalized damping matrix
$\hat{f}_a$ = generalized aerodynamic (CFD) load vector
$\hat{f}_I$ = generalized impulse force vector
K = elastic stiffness matrix
$\hat{K}$ = generalized stiffness matrix
M = inertia matrix
$\hat{M}$ = generalized inertia matrix
M_∞ = freestream Mach number
N = FE shape function
p = Euler pressure
$q, \dot{q}$ = generalized displacements and velocities
$\bar{q}$ = dynamic pressure
$u, \dot{u}$ = structural deformations and velocities
V = vector of fluids unknown variables
V_f = flutter speed index
ζ = damping
λ = flutter parameter
μ = viscosity
ρ = density
Φ = matrix of structural eigenvectors
ω = frequencies
ω_α = first torsional frequency

Introduction

MODERN, high-performance aerospace vehicles are characterized by unprecedented levels of multidisciplinary interactions of a number of major technical disciplines such as structures, aerodynamics, and controls engineering, among others, which may impose considerable constraint on dynamic stability and controls performance margins required for flight safety. Accurate prediction of such flight characteristics prior to flight testing is thus of vital importance to enable safe flight testing of new and modified advanced aircraft. Activities have been aimed at developing an integrated multidisciplinary analysis tool capable of accurate computation of flight critical dynamic stability and controls performance characteristics. In the design of such a computational tool, the choice of an appropriate methodology for modeling of the various solution domains as well as accurate simulation of the interaction of relevant forces at their respective boundaries is of utmost importance to ensure effective computation of aeroelastic phenomena in a routine fashion, when applied to the solution of complex practical problems.

A number of researchers have recently published results of their work in the application of computational fluid dynamics (CFD) to aeroelastic analysis involving unsteady flows. Thus, Ref. 1 summarizes such activities that utilize finite difference methods for the solution of lower-order CFD methods as the transonic small disturbance and the full potential equations in the aeroelastic analysis and also for effective flutter control.[2] Further work involving the finite difference solution of Euler and Navier–Stokes equations employing structured aerodynamic meshes that are coupled to finite element (FE) structural solution for aeroelastic analysis is presented elsewhere.[3,4] Extensive recent efforts in this connection using structured aerodynamic grids and a finite volume solution of Euler equations have also been reported.[5,6] Further extensions of this work employing unstructured meshes are described.[7,8] In particular Ref. 8 provides a detailed description of flutter analysis for some representative problems and compares such data with available experimental results. Also, a recent paper[9] presents an overview of application of these techniques to National Aerospace Plane (NASP) like hypersonic vehicles, whereas Ref. 10 provides an alternative approach to the solution of the aeroelasticity problem.

The analyses, as discussed previously, effect the simultaneous time-integration of the structural equations of motion with the governing flow equations for computation of unsteady aerodynamic forces. In such time-marching unsteady flow and aeroelastic calculations, the aerodynamic mesh needs to be updated at every time level, particularly for large structural deformations, so that it follows the deformed structural configuration. A deforming mesh algorithm has been described[7] that implements such a general mesh-updating procedure.

For complex aerospace vehicle configurations, it is necessary to adopt an accurate domain discretization procedure for effective idealization of these configurations. In this connection the finite element method (FEM) proves to be a viable technique to model both the fluids and solids continua and, therefore, is a natural choice for aeroelastic analysis that involves interaction of associated disciplines. An earlier effort involving FE CFD analysis for unsteady flow has been reported elsewhere.[11] This article presents details of a unified

Received May 8, 1995; revision received March 15, 1996; accepted for publication April 30, 1996.

*Aerospace Engineer. Member AIAA.

FE-based nonlinear aeroelastic analysis procedure as well as the resulting multidisciplinary analysis code STARS.[12] The primary elements of this approach include FE structural, heat transfer, and CFD analysis procedures, three-dimensional unstructured fluids grid generation capability, and a solids–fluids interface modal data and pressure interpolation program.

Some numerical results are also presented that demonstrate the accuracy and efficacy of the STARS computer program. The first example relates to a rectangular panel with clamped edges, and the STARS nonlinear flutter solution is compared with that obtained by linear analysis as well as wind-tunnel tests. An isolated, 45-deg swept-back wing is chosen as the second example, and relevant flutter solution results are compared with experimental data for a range of freestream Mach numbers that define the flutter boundary.

Description of Numerical Techniques and Software

A number of consistent disciplines and innovative algorithms have been incorporated into an integrated system designed to simulate aeroelastic performance characteristics of advanced aerospace vehicles. Since the FE technique can be commonly utilized to discretize relevant solids and fluids continua, its employment ensures accurate interaction of the related disciplines. Also, unstructured grid methodology, synonymous with the FEM, is a natural choice for accurate discretization of complex, practical solution domains. The STARS analysis package consists of a collection of highly integrated, general-purpose FE software developed for the solution of linear and nonlinear engineering problems spanning from single to multiple disciplines. Relevant details of the FE formulation of the individual key discipline areas as well as their interactions are summarized next.

FE Structural Analysis

The structural analysis module is capable of modeling and simulating complex structures with general boundary and mechanical as well as thermal loading conditions. Structural material properties may also be quite general including anisotropic ones, and the extensive program element library includes advanced layered composite and sandwich elements. Related data for temperature-dependent properties are stored in the material module of the program. A typical matrix numerical formulation representing a broad class of structural problems may be written as follows:

$$Kq + C\dot{q} + M\ddot{q} = f(t) \tag{1}$$

where K is the stiffness matrix and includes geometric stiffness matrix K_G and centrifugal force matrix K' for spinning structures; C is the viscous damping matrix and equals $C_c + C_d$ for the spinning case, C_c and C_d being the Coriolis and viscous damping matrices, respectively; and $f(t)$ being the externally imposed forcing function.

Static, stability, and dynamic analyses for linear and nonlinear structures may be effectively performed by this module. An efficient free vibration analysis of the appropriate form of Eq. (1) is vital for the computation of unsteady aerodynamic forces.

FE CFD Analysis

The dynamic behavior of a viscous, heat-conducting, compressible fluid obeying conservation of mass, momentum, and energy may be expressed by a set of partial differential equations

$$\frac{\partial \boldsymbol{V}}{\partial t} + \frac{\partial \boldsymbol{F}_i}{\partial x_i} = \boldsymbol{f}_b, \qquad i = 1, 2, 3 \tag{2}$$

where the solution, flux, and body forces column vectors as well as the viscous stress tensor are defined as

$$\boldsymbol{V} = \{\rho \quad \rho u_j \quad \rho E\} \tag{3}$$

$$\boldsymbol{F}_i = \left\{\rho u_i \quad \rho u_i u_j + p\delta_{ij} + \sigma_{ij} \quad u_i(p + \rho E) + u_j\sigma_{il} + k\frac{\partial T}{\partial x_i}\right\} \tag{4}$$

$$\boldsymbol{f}_b = \{0 \quad f_{bj} \quad u_i f_{bi}\} \tag{5}$$

$$\sigma_{ij} = -\frac{2}{3}\mu\frac{\partial u_k}{\partial x_k}\delta_{ij} + \mu\left(\frac{\partial u_i}{\partial x_j} + \frac{\partial u_j}{\partial x_i}\right) \tag{6}$$

in which ρ, p, and E are the density, average pressure intensity, and total energy, respectively; δ_{ij} is the Kronecker delta; u_j is the velocity component in the direction x_j of a Cartesian coordinate system; k is the thermal conductivity; and f_b represents body forces. The previous equations are supplemented with the state equations

$$p = (\gamma - 1)\rho(E - \tfrac{1}{2}u_i u_i) \tag{7}$$

$$T = (E - \tfrac{1}{2}u_i u_i)c_v \tag{8}$$

for a complete solution, in which γ is the ratio of specific heats and c_v is the specific heat at constant volume, such a formulation being valid for a perfect gas. A solution of the nonviscous form of Eq. (2) may be achieved by first obtaining a Taylor series expansion of V in time domain. The spatial domain Ω is next discretized by unstructured meshes consisting of three-dimensional tetrahedron elements. Using linear, FE approximations, $V = N\hat{V}$, $\hat{V}$ and N being nodal variable values and the shape function, respectively, and employing a Galerkin weighted-residual procedure, a time-dependent form of the governing equations may be obtained as

$$M\delta\hat{V} = \boldsymbol{R}_v + \boldsymbol{R}_s \tag{9}$$

in which time is the only independent variable, M is the usual mass matrix, and the right-hand side vectors $\boldsymbol{R}_v$ and $\boldsymbol{R}_s$ are associated volume and surface integrals containing $\boldsymbol{F}_i$ as defined in Refs. 13 and 14.

Solution of the system of ordinary differential equations defined in Eq. (2) is achieved by an explicit time-stepping iterative scheme employing a Taylor expansion of the solution $V(x_i, t)$ until steady conditions are achieved.[14,15] Since the computed solution V^{n+1} is expected to show oscillations in the vicinity of high gradients in flow phenomena such as shocks, it is smoothed at such locations by the introduction of appropriate artificial viscosity before proceeding to the next time step.[15] This scheme may further be augmented by a suitable flux-corrected transport (FCT) algorithm to achieve enhanced definition of discontinuities. Further improvement[16] of the Euler solution has been effected by implementing an Aitken acceleration technique. In this procedure, a solution variable result is sampled at three successive discrete time steps, and the Aitken technique is then used to obtain a revised estimate of the solution. Furthermore, the computer program developed in connection with the work presented in Ref. 17, which is also utilized for some of the present work, employs an FE multigrid solver for the efficient solution of Euler equations.

An advancing front technique, developed for automated three-dimensional unstructured mesh generation has been found to be rather suitable for discretization of complex solution domains. Such an algorithm was initially developed[18] for arbitrary, multiconnected, planar domains in which the interior nodes are generated first, which are then suitably linked to yield the best possible triangulation; during this process, the generation front is continually updated each time a new element is constructed. Further improvement and extension of this technique in three dimensions are described elsewhere,[13] in which the nodes and triangles are formed simultaneously for all boundary surfaces. This is followed by generation of tetrahedra by the advancing front approach to fill the entire solu-

tion domain. Suitable background grids are utilized to specify important mesh parameters defining node spacing, stretching parameters, and directions.

The three-dimensional automated unstructured mesh generation scheme, as described previously, has been found to be rather versatile for the modeling of a practical CFD solution domain around a complex structural form such as an aircraft. However, since the advancing front technique involves a rather extensive search for nodes and faces on the front, the grid generation time tends to be rather large for complex configurations. A simple modification of the procedure, implemented during our current effort, proves to be rather efficient and economical. In this procedure,[19] the usual technique is first utilized to generate a grid whose cells have a linear dimension about twice the desired size, and then each cell is reduced locally to reach desired cell sizes. Such a subdivision is effected by introducing the midpoint of each edge of an original triangle as a new grid point and connecting the three midpoints with line segments; in the particular case of a triangle side lying on a boundary edge, the midpoint of that edge is actually obtained by interpolation from the respective cubic curve defining that edge. Similarly, each tetrahedral cell of the three-dimensional grid is replaced by eight new cells by introducing six new nodes at the midpoint of each edge and connecting them appropriately with line segments; thus, each tetrahedron is one-eighth volume of the original tetrahedron.

Flutter and Aeroservoelastic Analysis

An effective aeroservoelastic (ASE) analysis module was implemented earlier for linear systems[20] in the STARS program in which panel methods are used for the computation of unsteady aerodynamic forces. For the nonlinear case, a somewhat different approach is needed to evaluate the aero-structural-controls interaction in an aerospace vehicle.

Thus, a steady-state Euler solution is first effected in which optimum solution convergence is achieved through an explicit, local time-stepping solution procedure that also employs a residual smoothing strategy. The FE structural model is then used to compute the natural frequencies ω and modes ϕ that consist of rigid body, elastic, and control surface motions, by solving

$$M\ddot{u} + Ku = 0 \tag{10}$$

in which u is the displacement vector. This is achieved by an efficient block Lanczos procedure that fully exploits matrix sparsity.[21,22] The resulting vehicle equation of motion is then cast into the frequency domain as follows:

$$\hat{M}\ddot{q} + \hat{C}\dot{q} + \hat{K}q + \hat{f}_a(t) + \hat{f}_l(t) = 0 \tag{11}$$

in which the generalized matrices and vectors are as follows: q is the displacement vector ($=\Phi^T u$); $\hat{f}_a(t)$ is the aerodynamic (CFD) load vector ($=\Phi^T \Sigma\, pA$); p is the Euler pressure at a node and A is the appropriate surface area around the node; and $\hat{f}_l(t)$ is the impulse force vector ($=\Phi^T f_l$) (where $\hat{f}_l$ is the user input that contains a number of modes of interest). The vector $\hat{f}_a$ may be generated from nodal pressure values of the FE structural grid that are in turn computed by interpolation from such values at aerodynamic grid points derived from a CFD Euler solution. In this process, for each structural node pertaining to an element, a triangular aerodynamic element encircling the node is first identified. Then, contribution of the

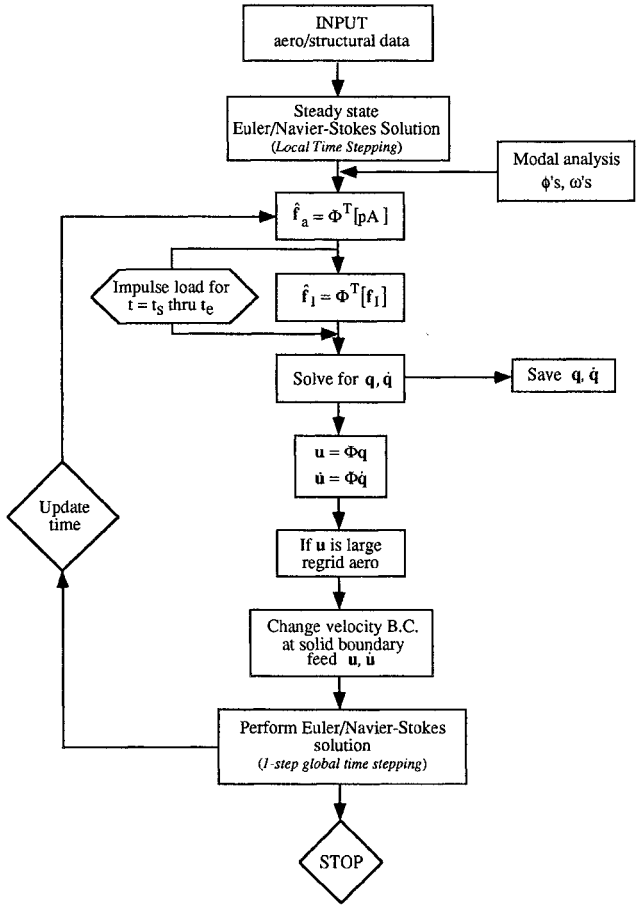

Fig. 1 Flowchart for STARS nonlinear aeroelastic and flutter analysis.

Table 1 Natural frequencies and flutter parameters of rectangular panels

	Frequencies, Hz	
Mode	4 × 1 panel	2 × 1 panel
1	12.6334	14.7965
2	14.8410	23.5866
3	18.5320	38.3150
4	23.7127	50.3578
5	30.3829	58.9320
6	38.5394	59.0684
	Flutter parameter	
STARS	4.01	5.03
Ref. 23	4.18	5.30

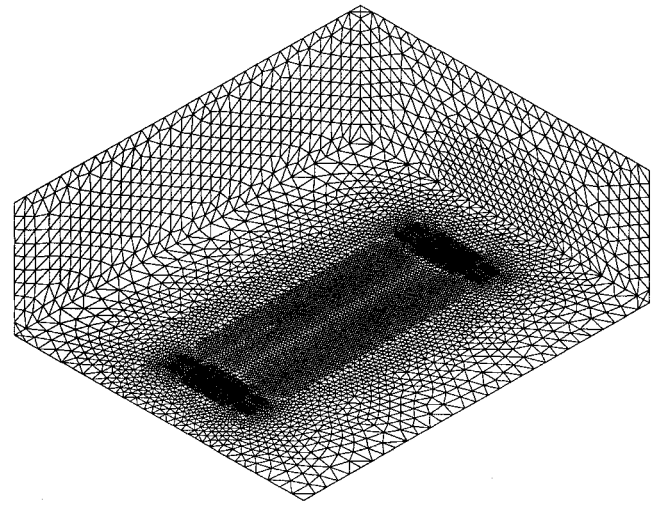

Fig. 2 Aerodynamic surface grids of a rectangular panel and the computational domain.

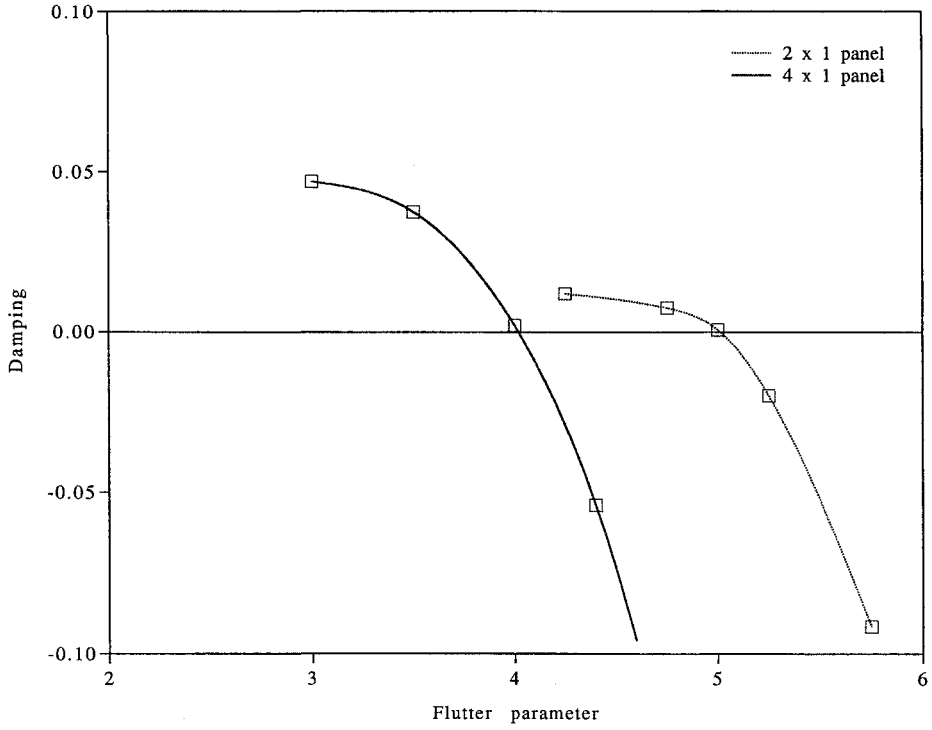

Fig. 3 Damping plots for the rectangular panels at Mach 3.0.

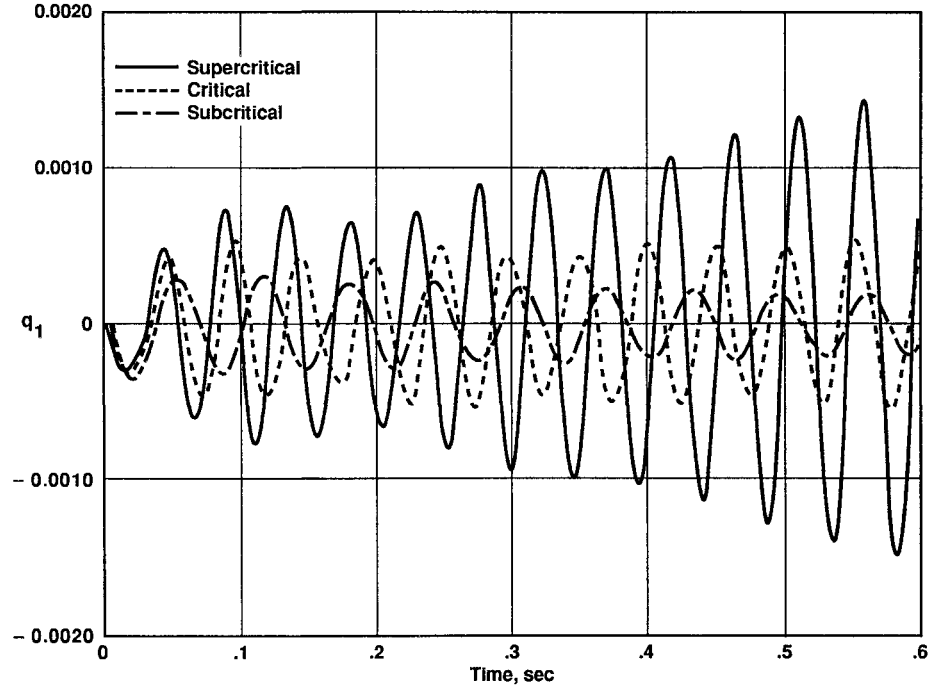

Fig. 4 First generalized displacement plots for the 4 × 1 panel at various values of the flutter parameter.

aerodynamic nodal values to the structural node is computed by standard FE interpolation procedures employing the relevant element shape function N. This process is repeated for the rest of the structural nodes to yield nodal aerodynamic pressure values from which the generalized forces are derived by standard modal transformation. Alternatively the modal vectors pertaining to aerodynamic nodes on structural surfaces Φ_a is derived first from Φ, again by using the appropriate N, and the Euler nodal pressures are next used directly to obtain $\hat{f}_a$; this approach has been implemented in the current analysis.

Equation (11) may next be formulated in the state–space matrix equation form as

$$\dot{X} = AX + b_a(t) + b_l(t) \tag{12}$$

where

$$X = \begin{bmatrix} q \\ \dot{q} \end{bmatrix}$$

$$A = \begin{bmatrix} 0 & I \\ -\hat{M}\bar{V}^{1}\hat{K} & -\hat{M}\bar{V}^{1}\hat{C} \end{bmatrix}$$

$$\boldsymbol{b}_a(t) = \begin{bmatrix} 0 \\ -\hat{M}^{-1}\hat{\boldsymbol{f}}_a(t) \end{bmatrix}$$

$$\boldsymbol{b}_I(t) = \begin{bmatrix} 0 \\ -\hat{M}^{-1}\hat{\boldsymbol{f}}_I(t) \end{bmatrix}$$

and a time response solution of Eq. (12) in an interval Δt ($=t_{n+1} - t_n$) is obtained as

$$\boldsymbol{X}_{n+1} = e^{A\Delta t}\boldsymbol{X}_n + A^{-1}[e^{A\Delta t} - I][\boldsymbol{b}_a(t_n) + \boldsymbol{b}_I(t_n)] \quad (13)$$

Such data consisting of $\boldsymbol{q}$ and $\dot{\boldsymbol{q}}$ vectors are next stored for later processing. The structural deformations $\boldsymbol{u}$ and velocities $\dot{\boldsymbol{u}}$ are then computed from $\boldsymbol{q}$ and $\dot{\boldsymbol{q}}$, respectively, and the aerodynamic mesh is updated only if large motions are encountered. Such $\boldsymbol{u}$ and $\dot{\boldsymbol{u}}$ values are next input into the CFD code to change velocity boundary conditions at the solid boundary. This is then followed by a one-step Euler solution using a global time-stepping scheme, and the entire solution process is then repeated for the required number of time steps.

The response data, as previously shown, may next be resolved into modal components utilizing a fast Fourier transform:

$$\boldsymbol{q} = \sum_{m=1}^{r} e^{\zeta_m t}(a_m \cos \omega_m t + b_m \sin \omega_m t) \quad (14)$$

yielding the ζ and ω values. This process is repeated for a number of dynamic pressure values, $\bar{q} = \frac{1}{2}\rho V^2$ and the ζ and ω values plotted against the Mach number; V is the freestream velocity. Such a plot depicting stability characteristics of the vehicle enables the prediction of the onset of flutter or divergence occurring within the entire flight regime. Figure 1 shows

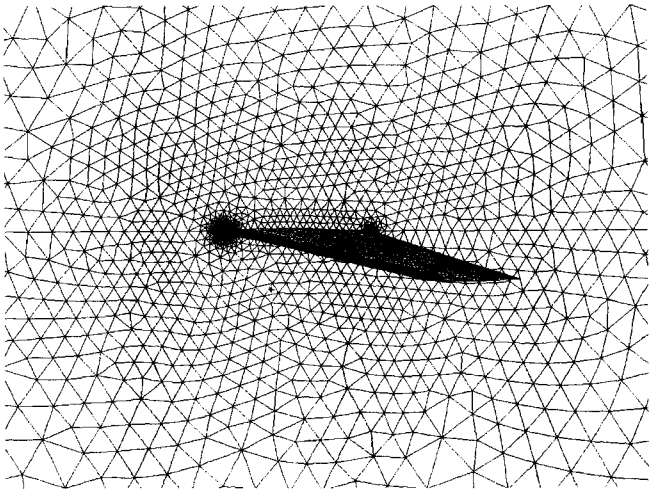

Fig. 5 Partial view of CFD surface grid for the AGARD wing and the symmetry plane.

Table 2 Comparison of calculated and experimental flutter solutions for the AGARD wing 445.6

Freestream	Flutter speed index			
M	STARS	Ref. 6	Ref. 8	Test, Ref. 24
0.499	0.436	0.439	0.43	0.446
0.678	0.380	0.417	0.40	0.417
0.900	0.341	0.352	0.31	0.370
0.960	0.280	0.275	0.23	0.308
1.072	0.302	0.466	——	0.320
1.141	0.410	0.660	——	0.403
		(0.466, Ref. 26)		
	Flutter frequency ratio			
0.499	0.477	0.597	0.52	0.535
0.678	0.428	0.539	0.47	0.472
0.900	0.397	0.425	0.37	0.422
0.960	0.364	0.343	0.31	0.365
1.072	0.363	0.541	——	0.362
1.141	0.435	0.764	——	0.459
		(0.47, Ref. 26)		

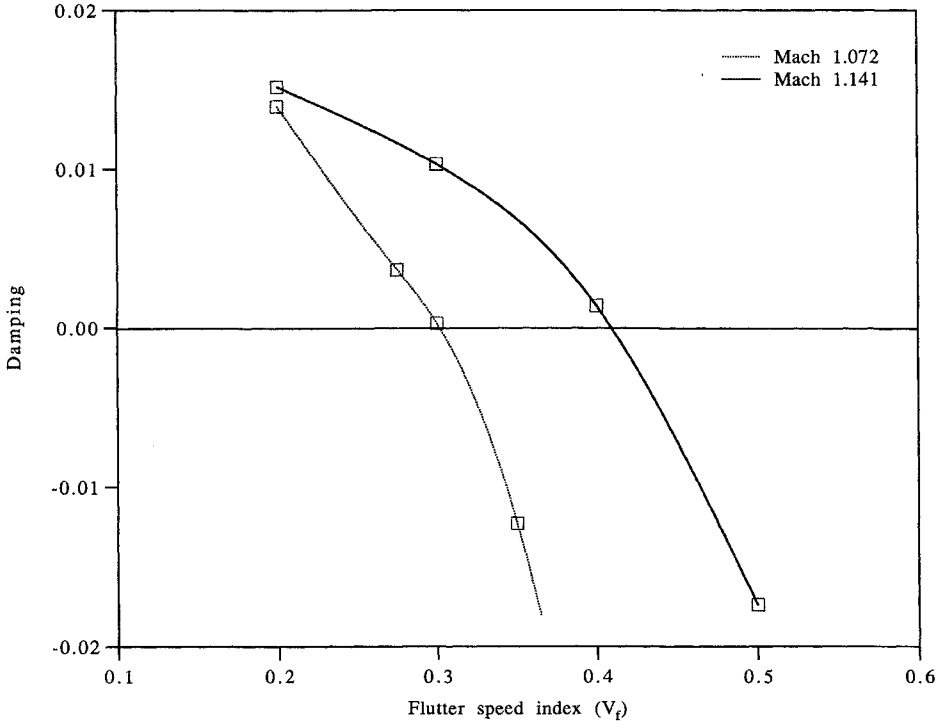

Fig. 6 Damping plots for two typical Mach numbers for the AGARD wing.

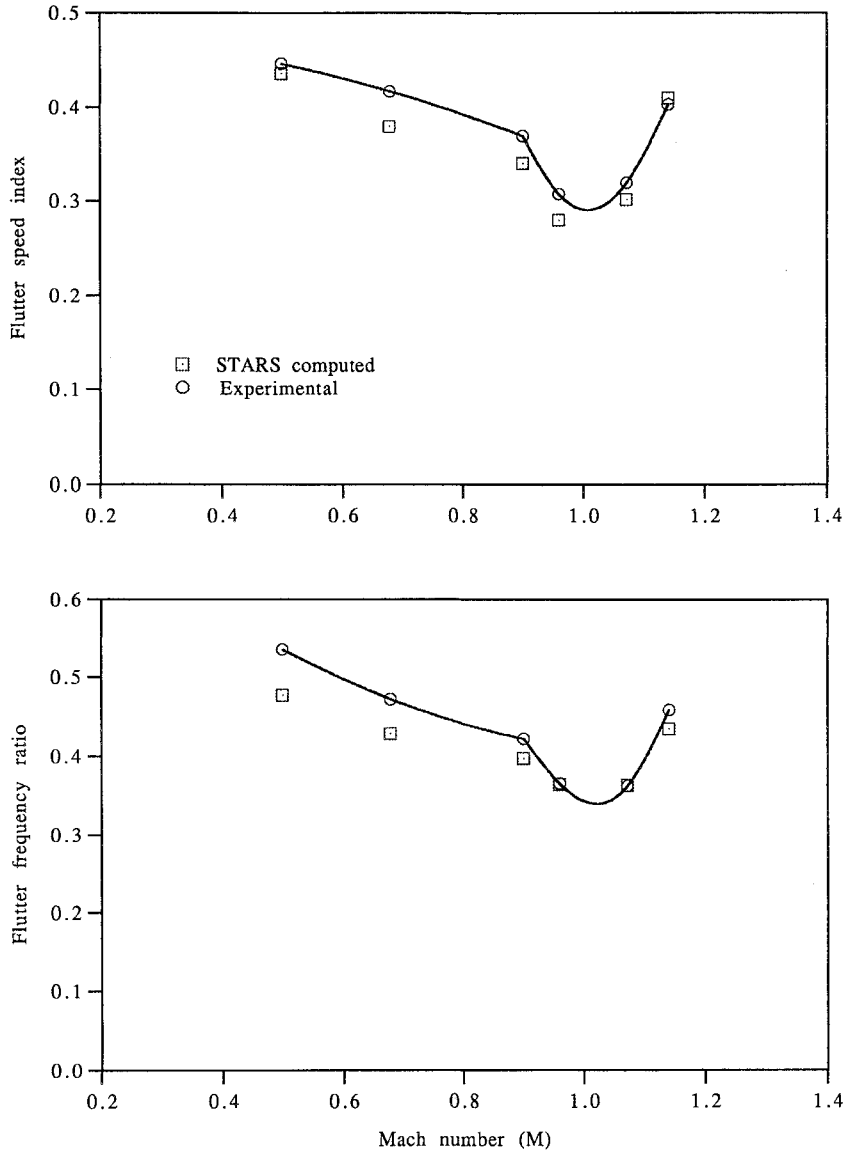

Fig. 7 Comparison of STARS flutter predictions with experimental results for the AGARD wing.

a flowchart of the related numerical algorithm adopted in the STARS program.

Numerical Examples

A number of relevant numerical example problems have been solved to assess the efficacy of the currently developed numerical algorithms and tools. Examples of flutter analysis of some representative test problems are presented next.

Rectangular Panel

Reference 23 provides details of extensive flutter calculations for a rectangular panel employing approximate aerodynamic theory, and such results are also compared with experimental findings. The STARS CFD and ASE modules were used to perform nonlinear flutter analysis of the simply supported panel for aspect ratios of 2 and 4, respectively. Figure 2 depicts an open view of the aerodynamic surface grids of the 4 × 1 panel and inside surfaces of the solution domain. The associated three-dimensional CFD grid consists of 45,371 nodes and 239,109 tetrahedral elements, which was used for both steady and unsteady aerodynamic calculations. While the structural mesh on the plate surface consists of 800 triangular elements, the corresponding aerodynamic mesh employs 3512 such elements. The first six modes Φ were used for the aeroelastic analysis, and the computed natural frequencies ω are given in Table 1 for both plates. Such modal values, pertaining to the plate surface aerodynamic grid Φ_a are obtained by suitable interpolation from corresponding structural nodal data. Typical structural and aerodynamic basic data adopted for the analysis are given as follows:

Poisson's ratio ν = 0.3
Young's modulus E = 0.6894E+11
Panel density = 2750.0
Panel thickness t = 0.005
Mach number M_∞ = 3.0

A series of aeroelastic analyses was performed for a number of dynamic pressure values to locate the flutter speed; the calculated damping values are plotted in Fig. 3 against varying flutter parameter values, $\lambda^{1/3}b/a$, in which

$$\lambda = \frac{2\bar{q}a^3}{\beta D}$$

where

$$\beta = \sqrt{M_\infty^2 - 1}$$

$$D = \frac{Et^3}{12(1 - \nu^2)}$$

A positive damping signifies convergence of the generalized displacements and velocities, whereas solution divergence is indicated by its negative value.

Table 1 also presents a comparison of STARS calculated panel flutter solution results with that presented in Ref. 23, the latter having been verified by experimental means. Also, Fig. 4 shows plots of the time history of the first generalized displacement pertaining to subcritical, critical, and supercritical values of the dynamic pressure for the 2 × 1 panel that corresponds to flutter parameter values of 4.25, 5.0, and 5.25, respectively. The nondimensional global time step was taken as 0.001297 for the 4 × 1 panel, which was further subdivided into 40 substeps for time-marching calculations, and the CPU time per cycle of calculation for the dominant flutter mode was found to be about 11.13 h using an IBM RS6000/590 workstation. On average, about four to six cycles need to be computed, at every specific value of dynamic pressure, to establish a clear pattern of solution convergence.

AGARD 45-Deg, Swept-Back Wing 445.6

The wing is an AGARD standard aeroelastic configuration with a 45-deg, quarter-chord sweep angle, a panel aspect ratio of 1.65, a taper ratio of 0.66, and a NACA 65A004 airfoil section. Measured modal frequencies and wind-tunnel flutter test results of the wing are detailed elsewhere[24,25]; the model selected for analysis and correlation is referred to as the 2.5-ft weakened model 3.

An FE model of the wing yielded natural frequencies and mode shapes, similar to those derived experimentally.[24,25] The first four modes represent first bending, first torsion, second bending, and second torsion, respectively, the corresponding frequencies in Hz being 9.60, 38.20, 48.35, and 91.54, respectively. These data were used for subsequent aeroelastic analysis to obtain flutter characteristics of the wing at freestream Mach numbers 0.499, 0.678, 0.901, 0.960, 1.072, and 1.140, respectively, to effect comparison with test results as well as that derived in Refs. 6 and 8, based on the Euler solution by the finite volume method and also Ref. 26 that extended this analysis[6] to viscous flow. To bracket the flutter points, for each Mach number, a set of aeroelastic responses was computed for several values of dynamic pressure. Figure 5 shows the partial view of the CFD grid on the surface of the wing and the symmetry plane; an associated three-dimensional CFD grid consists of tetrahedral fluid elements. The following details pertain to a typical solution for each flutter point using the IBM RS6000/590 workstation:

Number of nodes in CFD grid	= 45,180
Number of CFD elements	= 240,373
Global time step Δt	= 0.0017027
Number of steps/cycle for the dominant mode	= 4167
CPU time/cycle for the dominant flutter mode	= 19.65 h
Number of cycles per flutter point	= 4–6

The calculated global time step was further subdivided into 40 substeps to facilitate time-marching calculations. For supersonic flow, an enhanced grid, consisting of 69,630 nodes and 373,798 elements, was used for the respective solutions; the CPU time for each cycle of unsteady analysis was about 31.75 h. A structural damping coefficient of 0.02 has been used for all test cases.[25] Figure 6 shows computed damping results against flutter speed index values for two Mach numbers. Furthermore, it may be noted that for subsonic cases, further refinement of the aerodynamic grid did not show any significant improvement in the solution result and therefore was not needed; in the supersonic case, however, the mesh had to be further refined to yield more accurate results.

Table 2 presents a comparison of flutter solution results obtained by the STARS FE aeroelastic analysis, wind-tunnel test[24,25] and the finite volume procedures employing structured[6,26] and unstructured[8] grids, respectively; such results for viscous flow[26] show improvement in solution accuracy for the Mach 1.141 case. These results are further depicted in Fig. 7. While results quoted from Ref. 6 were available in tabular form, such results were extracted from graphical depiction of the same presented in Ref. 8. The associated V_f is defined as $V/(b_s\omega_\alpha\sqrt{\bar{\mu}})$, in which V is the stream velocity, b_s is the root semichord, ω_α is the first torsional frequency, and $\bar{\mu}$ is the mass ratio.[24]

Concluding Remarks

An integrated, FE-based, numerical methodology and associated computer code developed for effective modeling and simulation of aeroelastic behavior of aerospace structures have been presented. Adoption of the common FEM effects accurate transfer of data from fluids to structural domain and vice versa, thereby ensuring accurate representation of their interaction phenomenon.

Flutter solutions for the rectangular panel indicate close agreement between analysis and test results as shown in Table 1. Such results for the AGARD 45-deg swept-back wing present interesting data on relative efficacies of the various solution procedures. Thus, Fig. 7, depicting STARS analysis and test results,[24] shows good correlation both in subsonic and transonic/supersonic regimes. Table 2 provides, in tabular form, a comparison of flutter test data,[24] with STARS FE and also finite volume analyses employing structured[6] and unstructured[8] grids, respectively. While all three analysis results correlate rather well in the subsonic area, the current analysis technique also provides excellent correlation with test results in the flow regime where Mach number is above unity. Furthermore, the computer CPU time per cycle of STARS unsteady flow calculation was found to be similar to that in Ref. 8.

All analyses were performed on commonly available workstations. Thus, the STARS program is capable of performing routine aeroelastic analysis of practical problems at a relatively moderate cost, without having to use supercomputers that are not usually available to an average analyst.

Acknowledgments

The author would like to thank E. Hahn, C. Bach, T. Walsh, and other members of the STARS engineering group for their extensive effort in the preparation of the example problems. Thanks also go to J. Peraire of the Massachusetts Institute of Technology and A. Arena of Oklahoma State University for valuable assistance in the development of this work.

References

[1]Edwards, J. W., and Malone, J. B., "Current Status of Computational Methods for Transonic Unsteady Aerodynamic and Aeroelastic Applications," NASA TM-104191, Dec. 1991.

[2]Ide, H., and Shankar, V. J., "Unsteady Full Potential Aeroelastic Computations for Flexible Configurations," AIAA Paper 87-1238, June 1987.

[3]Guruswamy, G. P., "Time-Accurate Unsteady Aerodynamic and Aeroelastic Calculations of Wings Using Euler Equations," AIAA Paper 88-2281, April 1988.

[4]Guruswamy, G. P., "Vortical Flow Computations on a Flexible Blended Wing-Body Configuration," *AIAA Journal*, Vol. 30, No. 10, 1992, pp. 2497–2503.

[5]Robinson, B. A., Batina, J. T., and Yang, H. T. Y., "Aeroelastic Analysis of Wings Using the Euler Equations with a Deforming Mesh," *Journal of Aircraft*, Vol. 28, No. 11, 1991, pp. 781–788.

[6]Lee-Rausch, E. M., and Batina, J. T., "Wing Flutter Boundary Prediction Using Unsteady Euler Aerodynamic Method," NASA TM-107732, March 1993.

[7]Batina, J. T., "Unsteady Euler Algorithm with Unstructured Dynamic Mesh for Complex-Aircraft Aerodynamic Analysis," *AIAA Journal*, Vol. 29, No. 3, 1991, pp. 327–333.

[8]Rausch, R. D., Batina, J. T., and Yang, H. T. Y., "Three-Dimensional Time-Marching Aeroelastic Analyses Using an Unstructured-Grid Euler Method," *AIAA Journal*, Vol. 31, No. 9, 1993, pp. 1626–1633.

[9]Ricketts, R. H., Noll, T. E., Whitlow, W., and Huttsell, L. J., "An Overview of Aeroelasticity Studies for the National Aero-Space Plane," AIAA Paper 93-1313, April 1993.

[10]Bendicksen, O. O., "A New Approach to Computational Aeroelasticity," AIAA Paper 91-0939, April 1991.

[11]Löhner, R., "Adaptive H-Refinement on 3-D Unstructured Grids for Transient Problems," AIAA Paper 89-0365, Jan. 1989.

[12]Gupta, K. K., "STARS—An Integrated General-Purpose Finite Element Structural, Aeroelastic, and Aeroservoelastic Analysis Computer Program," NASA TM-101709, June 1990; revised Dec. 1995.

[13]Peraire, J., Peiro, J., Formaggia, L., Morgan, K., and Zienkiewicz, O. C., "Finite Element Euler Computations in Three Dimensions," *International Journal for Numerical Methods in Engineering*, Vol. 26, No. 10, 1988, pp. 2135–2159.

[14]Donea, J., "A Taylor-Galerkin Method for Convective Transport Problems," *International Journal for Numerical Methods in Engineering*, Vol. 20, No. 1, 1984, pp. 101–119.

[15]Morgan, K., Peraire, J., and Peiro, J., "The Computation of Three-Dimensional Flows Using Unstructured Grids," *Computer Methods in Applied Mechanics and Engineering*, Vol. 87, No. 3, 1991, pp. 335–352.

[16]Gupta, K. K., Petersen, K. L., and Lawson, C. L., "On Some Recent Advances in Multidisciplinary Analysis of Hypersonic Vehicles," AIAA Paper 92-5026, Dec. 1992.

[17]Peraire, J., Peiro, J., and Morgan, K., "A 3-D Finite Element Multigrid Solver for the Euler Equations," AIAA Paper 92-0449, Jan. 1992.

[18]Lo, S. H., "A New Mesh Generation Scheme for Arbitrary Planar Domains," *International Journal for Numerical Methods in Engineering*, Vol. 21, No. 8, 1985, pp. 1403–1426.

[19]Gupta, K. K., Petersen, K. L., and Lawson, C. L., "Multidisciplinary Modeling and Simulation of a Generic Hypersonic Vehicle," AIAA Paper 91-5015, Dec. 1991.

[20]Gupta, K. K., Brenner, M. J., and Voelker, L. S., "Integrated Aeroservoelastic Analysis Capability with X-29A Comparisons," *Journal of Aircraft*, Vol. 26, No. 1, 1989, pp. 84–90.

[21]Parlett, B. N., and Scott, D. S., "The Lanczos Algorithm with Selective Orthogonalization," *Mathematics of Computation*, Vol. 33, No. 145, 1979, pp. 217–238.

[22]Gupta, K. K., and Lawson, C. L., "Development of a Block Lanczos Algorithm for Free Vibration Analysis of Spinning Structures," *International Journal for Numerical Methods in Engineering*, Vol. 26, No. 5, 1988, pp. 1029–1037.

[23]Dixon, S. C., "Comparison of Panel Flutter Results from Approximate Aerodynamic Theory with Results from Exact Inviscid Theory and Experiment," NASA TN D-3649, Oct. 1966.

[24]Yates, E. C., Jr., Land, N. S., and Foughner, J. T., Jr., "Measured and Calculated Subsonic and Transonic Flutter Characteristics of a 45° Sweptback Wing Planform in Air and in Freon-12 in the Langley Transonic Dynamics Tunnel," NASA TN D-1616, March 1963.

[25]Yates, E. C., Jr., "AGARD Standard Aeroelastic Configuration for Dynamic Response, Candidate Configuration I.—Wing 445.6," NASA TM-100492, Aug. 1987; also *Proceedings of the 61st Meeting of the Structures and Materials Panel* (Germany), AGARD-R-765, 1985, pp. 1–73.

[26]Lee-Rausch, E. M., and Batina, J. T., "Calculation of AGARD Wing 445.6 Flutter Using Navier-Stokes Aerodynamics," AIAA Paper 93-3476, Aug. 1993.